PERGAMON

Electrochimica Acta 46 (2001) 1793–1813

ELECTROCHIMICA Acta

www.elsevier.nl/locate/electacta

Electrochemical impedance study of initial lithium ion intercalation into graphite powders

Chunsheng Wang [a,*], A. John Appleby [a], Frank E. Little [b]

[a] *Center for Electrochemical Systems and Hydrogen Research, Texas Engineering Experiment Station, Texas A&M University, College Station, TX 77843-3402, USA*

[b] *Center for Space Power, Texas Engineering Experiment Station, Texas A&M University, College Station, TX 77843-3118, USA*

Received 5 July 2000; received in revised form 4 December 2000

Abstract

A Johnson Matthey 287 (JM 287) graphite powder disks sandwiched between two nickel screens was used as working electrodes in 1.0 M lithium hexafluorophosphate in mixed carbonate ester electrolyte. Their intrinsic impedance and lithium intercalation kinetics were determined using several different electrochemical impedance spectroscopy (EIS) protocols. The thermal stability of the electrolyte was similarly studied using a floating palladium wire working electrode. Studies at 25°C and 65°C show that a first high frequency depressed semicircle, a second depressed semicircle, and a sloping line in the low frequency range are respectively related to the initial formation of a solid electrolyte interface (SEI) film, the charge-transfer reaction, and lithium diffusion in graphite. The intrinsic resistance is in series with the reaction impedance and effectively increases the latter. The charge-transfer semicircle at the open-circuit potential moves to the low frequency range, whereas the semicircle associated with the freshly formed SEI film moves to high frequency range as lithium insertion proceeds. The passivating SEI film formed at 25°C slows down co-insertion of the electrolyte into graphite when the electrode is cycled at 65°C, which increases the cycle life of graphite at elevated temperature.

Keywords: Electrochemical impedance spectroscopy; Solid electrolyte interface; Electrochemical reaction kinetics; Intrinsic resistance; Cycle stability

1. Introduction

Graphite is a most commonly used intercalation anode for lithium-ion batteries because of its high capacity (more than 300 mAh/g), flat potential profile, and reasonable cost. However the capacity stability of graphite is sensitive to electrode operating temperature. The cycle life of graphite at room temperature has been shown to improve by pre-cycling it at a lower temperature [1], and the cycle life of graphite becomes reduced when it is cycled at elevated temperature [2]. The temperature of formation of the complex passivating film known as the solid electrolyte interface (SEI) on the graphite surface must therefore play an important role in helping to stabilize the intercalation electrode capacity as a function of temperature [3]. The less passivating SEI film formed at elevated temperature may decrease the conductivity of the graphite agglomerate, and reduce the reversible capacity [4] by decreasing the amount of available active materials and by slowing the kinetics of electrochemical lithium insertion–extraction. A quantitative study of differences in the formation of the passive layer as a function of temperature should therefore help in understanding the mechanism of capacity degradation.

* Corresponding author. Tel.: +1-979-845-2033; fax: +1-979-845-9287.

E-mail address: cswang@pop.tamu.edu (C. Wang).

0013-4686/01/$ - see front matter

Electrochemical impedance spectroscopy (EIS) is a very sensitive detector of interfacial change, and is therefore commonly used to investigate the kinetics of growth and other properties of SEI films formed at room temperature [5–7]. While published EIS Nyquist plots as a function of potential for graphite intercalation electrodes generally resemble each other, explanations for the first depressed high frequency semicircle differ. It has generally been believed that this semicircle is related to the SEI film [5,6]. However this does not explain how it appears before the electrode is initially charged to 0.8 V versus Li, before the SEI film is believed to form. In an EIS study of SEI growth rather than its initial formation, Barsoukov et al. [5] investigated initial Li intercalation below the potential plateau for SEI film formation at room temperature and at −20°C. Recently, Chang and Sohn attributed the first depressed high frequency semicircle to contact resistance between electrode particles and the current collector [7]. The special EIS protocols given here show that the first high-frequency depressed semicircle results from the SEI film, although it is also influenced by the electrode contact impedance [8]. However, a reasonable explanation as to why this semicircle appears before initially charging to 0.8 V versus Li is required.

The formation and growth of the SEI film on graphite at room temperature and at 65°C is investigated by in-situ EIS for the first time in the present work. Special EIS protocols were used to study on the electrochemical reaction resistance and intrinsic (i.e. physical) resistance change during initial Li insertion into graphite.

2. Experimental

2.1. Electrode and cell preparation

JM 287 graphite powder (Johnson Matthey, Inc.), with a particle size of about 15 microns and a BET surface area of 13.5 m^2/g was used as the intercalation anode material. Composite electrodes were prepared from a mixture of 92 wt% JM 287 (ca. 50 mg) with 8 wt% polyvinylidene fluoride between two nickel screen current collectors using 1-methyl-2-pyrrolidinone as the solvent. After drying overnight at 120°C, the electrode was pressed into a sandwich structure with a geometric surface area of 2.0 cm^2 (ca. 0.8 mm). The configuration of a typical electrode is shown in Fig. 1 [9]. Electrochemical measurements were conducted in a special four-electrode PTFE cell. Two lithium foils were used as both counter and reference electrodes, and a floating palladium wire was used as an another working electrode to monitor the stability of the electrolyte at elevated temperature. All potentials given are versus the Li/Li^+ reference electrode in the experimental electrolyte, which was 1.0 M lithium hexafluorophosphate ($LiPF_6$) in a 1:1 by volume ethylene carbonate (EC)-dimethylcarbonate (DMC) mixture (High Purity Lithium Battery Grade, Mitsubishi Chemical Company) unless otherwise specified in Fig. 5. Cells were assembled in an argon-filled glove box. Charge (lithium intercalation) and discharge (lithium extraction) characteristics were measured between +0.0 and +1.5 V at a constant current using an Arbin (College Station, TX) automatic battery cycler. The graphite sandwich electrode was charged/discharged on one side only, and the voltage across its two sides was used to monitor its overall internal contact resistance. During initial Li insertion at 65°C, a current of 5 mA DC current was passed through the electrode to obtain the intrinsic resistance of electrode.

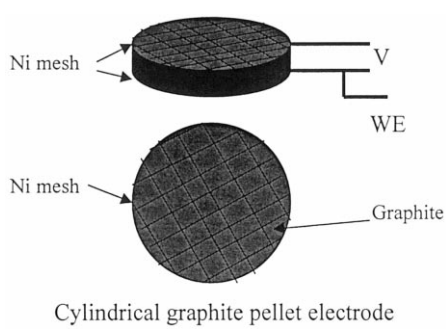

Fig. 1. Schematic diagram of graphite electrode configuration.

To avoid confusion concerning the various electrode resistances discussed here, the expression *intrinsic impedance* is used below to refer to those physical impedance elements of resistance present within the thickness of the electrode, excluding any electrochemical (faradaic) elements. They include the electronic impedance of the series-parallel array of graphite particles, the transmission lines of contact impedances between the particles (including ionic contacts and electronic contacts with and within the binder), and the electronic impedances of the current collectors and contact resistances between them and the neighboring graphite particles. This intrinsic impedance can be evaluated by an in situ EIS method.

2.2. EIS measurement

This was measured over the frequency range 65 kHz to 1.0 mHz at a potentiostatic signal amplitude of 5 mV, using a frequency response analyzer (Solartron, FRA 1250) and an electrochemical interface (Solartron, model 1286). EIS measurements were performed after 4 h of galvanostatic charging of freshly prepared JM 287 graphite electrodes, following a rest period of 10 h. Charging was at the 72 h full charge rate, based on an assumed maximum charge of 372 mAh/g. The potential

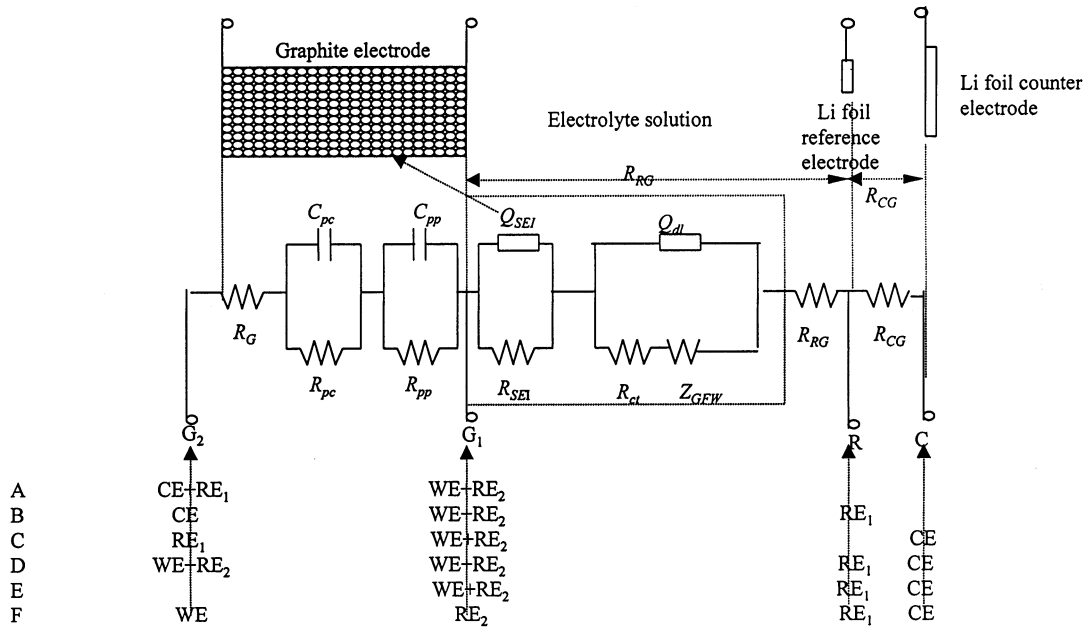

Fig. 2. Schematic diagram of cell and special Solatron electrochemical interface terminal-to-electrode connections. The suggested equivalent circuit for Li insertion–extraction into graphite electrode is also shown. R_G, R_{RG}, and R_{CG}: electronic graphite resistance, reference electrode to anode ionic resistance, and reference electrode to counter electrode ionic resistance. R_{pc}, R_{pp}, R_{SEI} and R_{ct}: graphite particles-to-current collector, particles-to-particles, SEI film, and charge-transfer resistances. C_{pc} and C_{pp}: particles-to-current collector and particles-to-particles contact capacitances. Q_{SEI} and Q_{dl}: constant-phase elements for the SEI film and for the double-layer respectively. Z_{GFW}: generalized finite Warburg element for lithium diffusion in graphite.

was recorded before each galvanostatic current interruption. For intrinsic resistance measurement, three intrinsic EIS scans were made using different methods for connecting the Solatron 1286 electrochemical interface terminals to the electrode. These were as follows:

1. between the two sides of the graphite electrode, connecting the RE_2 and WE terminals of the interface together to one of the sides, and RE_1 and CE to the other (called Protocol **A** in Section 3);
2. as (i), with RE_2 and WE connected to one side and CE to the other, with a lithium foil reference electrode connected to RE_1 (Protocol **B**);
3. with RE_2 and WE to one side and RE_1 to the other, with a lithium foil connected to CE as a counter electrode (Protocol **C**).

EIS measurements for the determination of electrochemical reaction kinetics were obtained using the following protocols:

1. with terminals RE_2 and WE connected to both sides of the electrode (Protocol **D**);
2. with terminals RE_2 and WE connected to one side only (Protocol **E**);
3. with terminal RE_2 to one side and terminal WE to the other (Connection **F**).

A schematic diagram of the cell and the different interface terminal-to-electrode connections, including the geometrical arrangement of the counter and reference electrodes for each protocol, is shown in Fig. 2. The differences between the three EIS scans thus obtained allow determination of the influence of contact resistance on electrochemical reaction kinetics. The manner in which the information is derived is described in a later section. Fitting of impedance spectra to the proposed equivalent circuit was performed by using the code Z_{view} (Version 1.4, Scribner Associates, Inc.).

3. Results and discussion

3.1. Capacity stability of JM 287 graphite cycled at 65°C

Aurbach et al. have reported that pre-cycling of graphite intercalation electrodes at low temperature improved their cycle life at room temperature [1]. They attributed this to a more advantageous SEI film formed at low temperature. To identify the effect of the SEI film first formed at room temperature on the cycling stability of graphite at elevated temperature, JM 287 graphite was cycled at 65°C with and without pre-cycling at 25°C, as shown in Fig. 3. The capacity of JM 287 graphite declined quickly to less than 40 mAh/g when it was cycled at 65°C. However, only a slow capacity decline at 65°C was observed in Fig. 3b when JM 287 was pre-cycled 17 times at 25°C. This result

shows that the SEI film preformed at room temperature can enhance the capacity stability of graphite at elevated temperature.

3.2. Initial charge–discharge behavior of JM 287 graphite at 25°C and 65°C

To investigate the influence of temperature on the formation of the SEI film, JM 287 electrodes were cycled at 25°C and 65°C. Charge–discharge curves for the first cycle are given in Fig. 4. When the charge had reached 200 mAh/g at 65°C, it was necessary to interrupt the 5 mA current passed through the electrode for intrinsic resistance measurement because the electrode conductivity became so low that a significant voltage difference was observed across the electrode. Under these conditions, the voltage across the electrode on charging/discharging on one side only was used to monitor the contact resistance. The results shown in Fig. 3 may be summarized as follows:

1. Cycling at elevated temperature causes an increase in irreversible capacity and in the potential for SEI film formation.

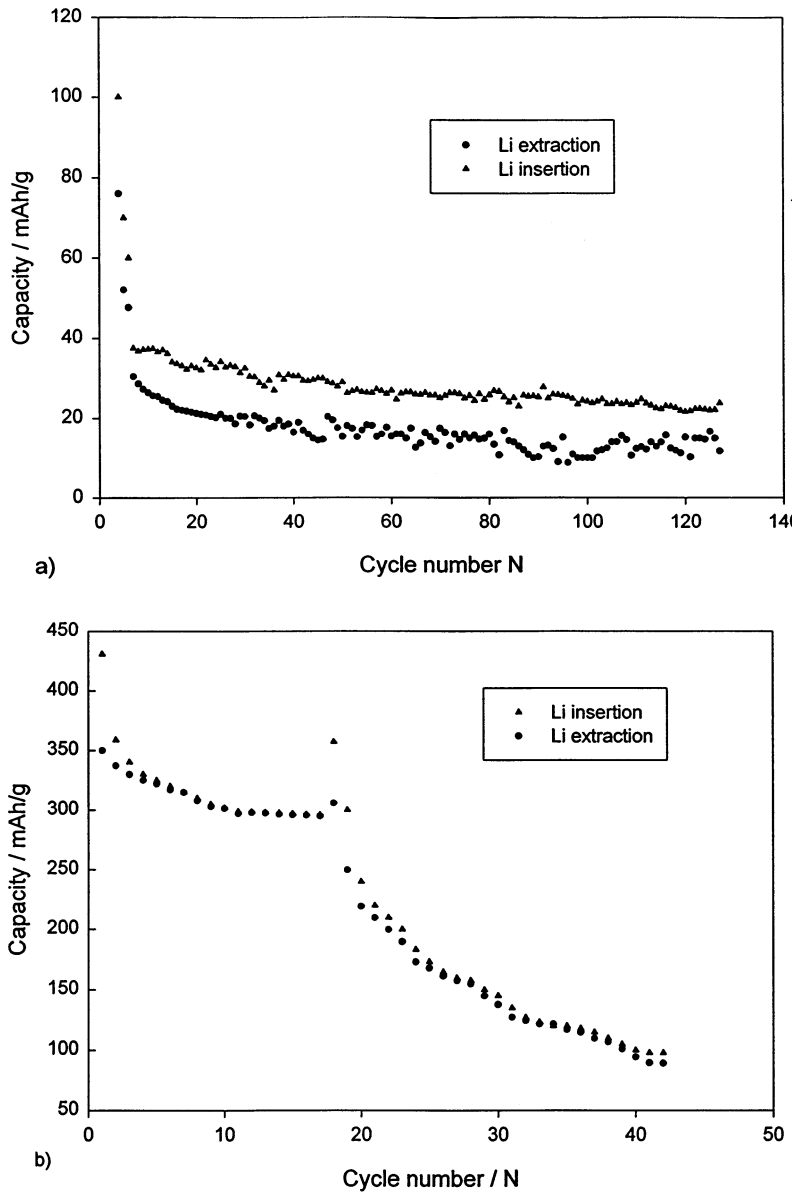

Fig. 3. Charge–discharge capacity versus cycle number for JM 287 graphite anodes. (a) Cycles at 65°C with cycling current of 6.5 mA/g. (b) After pre-cycling at 25°C for 17 cycles with further cycling at 65°C, with charge current of 5.1 mA/g.

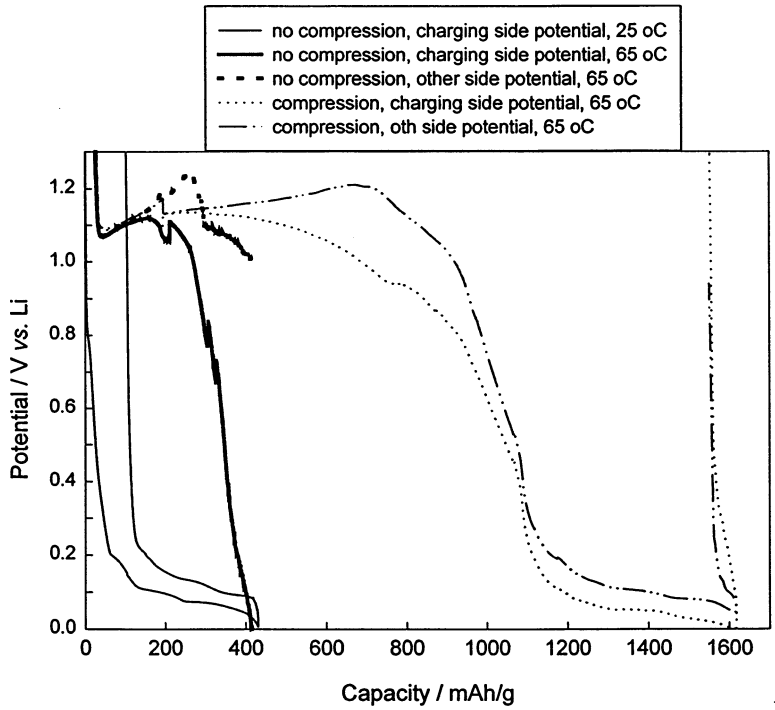

Fig. 4. Initial charge–discharge profiles for JM 287 graphite with current of 5 mA/g at 25°C and 65°C. In some cases, the JM 287 graphite anode was compressed between two PTFE holders with small holes to allow penetration of electrolyte.

2. During the initial insertion of Li into JM 287 at 65°C, the potential first decreased to 1.08 V and then increased to 1.12 V, showing that the rate of electrolyte reduction was faster than the rate of charging.

The high rate of electrolyte reduction may be caused by co-insertion of the electrolyte into graphite, giving an increase in voltage between the two sides of the electrode because of the contact resistance on charging on one side only. When the electrode was operated uncompressed, the voltage between the two sides of electrode could be as high as 1.0 V at the end of charge, while no potential plateau for Li insertion into graphite was observed. Finally the electrode broke up, resulting in electronic disconnection of graphite particles from the bulk. It was observed that much of the graphite was stripped from the Ni mesh substrate and fell to the bottom of the cell after the first cycle. Failure of graphite anodes due to disintegration with electronic disconnection has also been reported during initial Li insertion into graphite in PC [10] and PC-DMC (1:1.86) [11] solutions at room temperature. Thus, the performance of graphite electrodes in EC-DMC (1:1) at 65°C is similar to that in these electrolytes at room temperature. Compression of each side of the graphite electrode between two PTFE holders avoided the mechanical breakdown of the electrode, and gave a voltage difference of only 60 mV across the electrode at the end of charge at 0 V. Compression allows a greater quantity of graphite to become active, therefore to become involved in SEI film formation and in the co-intercalation of electrolyte. This increases the overall apparent charge capacity at potentials in excess of 0.2 V to more than 1100 mAh/g. Further charging to 0.2 V resulted in an additional 450 mAh/g, but only 10% of this was reversible. A probable explanation for this low reversible capacity is that continued SEI film growth (or electrolyte co-intercalation) occurs below 0.2 V because the film formed at 65°C is less passive [8].

Fig. 3 shows that the temperature at which initial SEI film formation occurs is critical in determining the cycling stability of graphite, and that EIS studies of the initial charging of JM 287 anodes at different temperatures are a convenient means of studying the phenomena involved.

3.3. Analysis of the first EIS (high-frequency) depressed semicircle

A correct interpretation of the Nyquist plots obtained is imperative if EIS is to be used as a diagnostic tool. The special EIS protocols were applied to JM 287 graphite anodes to determine if the first depressed semicircle (i.e. that at the highest frequency) is related

to the SEI film or to contact impedances between both graphite particles and the current collectors as Chang et al. [7] suggest.

In Fig. 2, R_G, R_{RG}, and R_{CG} are the electronic graphite resistance, the reference electrode to anode ionic resistance, and the reference electrode to counter electrode ionic resistance. R_{pc}, R_{pp}, R_{SEI} and R_{ct} are the graphite particles-to-current collector, particles-to-particles, SEI film, and charge-transfer resistances. C_{pc} and C_{pp} are the particles-to-current collector and particles-to-particles contact capacitances. Q_{SEI} and Q_{dl} are constant-phase elements for the SEI film and for the double-layer respectively, and Z_{GFW} is the generalized finite Warburg element for lithium diffusion in graphite. Here R_{SEI}/Q_{SEI} can be considered as three R/C circuits in series due to the SEI film of a multilayer structure, c.f., the similar equivalent circuit given by Levi and Aurbach [10].

From the arrangements in Fig. 2, it is clear that EIS obtained using Protocols **A** and **D** reflect the intrinsic graphite impedance and the graphite to electrolyte reaction impedance, respectively. The intrinsic impedance from Protocol **A** includes the electronic resistance of the series-parallel array of graphite particles, the transmission lines for the various contact resistances, viz. the current collector-to-particle impedances on one side, the particle-to-particle impedances through the electrode, and the particle-to-current collector impedances on the other side. The real parts of the arrays of electronic impedances for the graphite particles, for the particles-to-current collectors, and for particle-to-particle contact may be obtained from Protocol **A** EIS measurements by the intersections of the high-frequency line, and of the first and second semicircles, with the real axis, respectively [8,9]. The current corresponding to the electrochemical reaction of Li^+ using Protocol **D** must also go through the particle-to-particle, and particles-to-current collector arrays. Thus, the intrinsic impedance is in series with the reaction impedance, as is shown in the equivalent circuit of Fig. 2. The electrochemical impedance for Li insertion/extraction kinetics corresponds to two depressed semicircles with a low-frequency line for Li diffusion. The two depressed semicircles may be attributed to the impedance of the SEI film and to the charge-transfer reaction.

If the electrochemical interface terminal WE is disconnected from the G_1 side of the electrode, the EIS using Protocol **D** becomes that for Protocol **E**. The graphite particle to current collector distance in Protocol **E** is effectively double that of Protocol **D** whereas the particle-current collector area is halved. The contact impedance in series with the reaction kinetic EIS in Protocol **E** should then be twice that for Protocol **D**. If terminal CE is moved from lithium foil counter-electrode to G_2 side of electrode in Protocol **E**, the EIS will become that for Protocol **B**. The transelectrode Li charge–discharge current in Protocol **E** is replaced by an electronic transelectrode current in Protocol **B**. Hence, the EIS using Protocol **B** will be that for the intrinsic impedance involved in the kinetic EIS using Protocol **E**, minus the electrochemical kinetic impedance. Similarly, the EIS using Protocol **E** will becomes that using Protocol **C** if terminal RE_1 is moved from the Li reference electrode to the G_2 side of the graphite electrode. In protocol **C**, the transelectrode Li charge–discharge AC current is induced an AC voltage of 5 mV amplitude. Therefore the EIS using Protocol **C** also reflects the intrinsic impedance involved in the EIS obtained using Protocol **E**. The intrinsic impedance in series with the reaction kinetic EIS in Protocol **E**, which can be measured by EIS using Protocol **B** and **C**, should be half of that measured using Protocol **A**. This may be explained as follows. In Protocol **E**, the electrochemical reaction current generated from graphite particles at the closer (G_1) side must go through the interposed graphite particles and through one particles-to-current collector boundary. However, the electrochemical current generated from the particles on the G_2 side must pass through the electrode thickness before being collected through the particles-to-current collector contact. Therefore the average intrinsic impedance series with the reaction kinetic EIS in Protocol **E** is half of the overall electronic impedance of the series-parallel array of graphite particles, the particle-to-particle contact resistance transmission line, plus the particles-to-current collector contact impedance. As stated earlier, the intrinsic resistance measured from Protocol **A** includes the entire electronic resistance of the series-parallel array of graphite particles, with that of the transmission line for the various contact impedances, i.e. the current collector-to-particles on one side, particle-to-particle, and the particles-to-current collector on the other side. If the particle-to-current collector impedances are similar for each side, then the intrinsic impedances measured using Protocols **B** and **C** should be equal to half of that using Protocol **A**. Finally, the intrinsic resistance should not be present in Protocol **F** (see Fig. 2) because it automatically eliminates the intrinsic resistance of the graphite electrode.

The following results can therefore be expected from the six EIS protocols:

1. The intrinsic resistance using Protocol **B** should equal to that using Protocol **C**, but half of that using Protocol **A**.
2. The intrinsic resistance for Protocol **F** is zero, whereas that for Protocol **D** should be half of that for Protocol **E**. Therefore the EIS spectra for Protocol **D** should lie between those for Protocol **E** and **F**, since the intrinsic impedance is in series with reaction EIS (Fig. 2).

3. The impedance using Protocol **E** should be equal to the sum of the impedances using Protocols **F** and **B** (or **C**).

Fig. 5 shows the results of the six protocols for intrinsic and kinetic impedance measurements at 80 mV vs. Li/Li^+ on two JM 287 graphite electrodes. As expected, results on these two samples show that:

1. The impedance measured using Protocol **D** lies mid-way between those obtained using Protocols **E** and **F**.
2. The impedance measured using Protocol **E** is equal to the sum of the impedances using Protocols **F** and **B** (or **C**).
3. The intrinsic resistance measured using Protocol **B** is almost equal to that using Protocol **C**, 40–50% of that using Protocol **A**, the disparity being attributable to differences in contact impedance between the two sides of the electrode.

The results in Fig. 5 strongly suggest that:

1. The intrinsic impedance associated with the reaction kinetic EIS can be measured using Protocols **B** and **C**.
2. About the half of total intrinsic resistance is in series with the reaction kinetic EIS.
3. The first depressed semicircle is associated with the SEI film, although its value is also influenced by the electrode contact impedance. The reason for this is as follows.

If the first EIS depressed semicircle in kinetic impedance measurement is to graphite particle-to-current collector contact, the diameter of the first semicircle using Protocol **E** should be twice that for Protocol **D** (Fig. 2). This follows because the graphite particle-current collector area is doubled in the latter. In addition, the first semicircle should then not be present in Protocol **F**, since it automatically eliminates the intrinsic resistance of the electrode. However, the kinetic impedance results in Fig. 5 show that the first depressed semicircle is present in the Protocol **F** EIS, and is smaller than that for Protocol **D.** The first semicircle for Protocol **D** lies mid-way between those for **F** and **E**, but is not half of the size of that for Protocol **E**, as would be expected from Ref. [7].

To investigate SEI film formation and co-insertion of the electrolyte into graphite as a function of temperature, EIS of JM 287 electrodes was conducted during the first intercalation half-cycle at 25°C and 65°C. Electrode compression is important in determining the irreversible capacity in the first cycle at 65°C (Fig. 3), and commercial Li-ion electrodes are compressed. The JM 287 graphite anode used for EIS measurement was therefore compressed on each side by two PTFE holders containing small holes to allow penetration of electrolyte.

3.4. EIS measurements on JM 287 anodes during the initial charge at 25°C

Fig. 6 shows the potential measured at the end of each charge current pulse (4 h, corresponding to 6.5 mAh/g) and the apparent characteristic frequency as a function of charge capacity. The apparent characteristic frequency is defined by the frequency at the highest imaginary point of each semicircle. After 10 h relaxation time for each current pulse, EIS protocols A and D were used for intrinsic impedance and lithium insertion–extraction kinetic measurement, respectively. Fig. 7a shows the reaction kinetics impedance measurement at different Li content. Fig. 7b and c show selected Nyquist plots for reaction kinetic and intrinsic impedances at the Li insertion levels specified in Fig. 6. The change in potential for JM 287 using the pulsed charging currents shown in Fig. 6 was similar to the potential change using continuous galvanostatic charging at 25°C shown in Fig. 4. However, the charge capacity in the former case was higher than that in the latter. This is in agreement with previous results, i.e. the use of a low charging current increases irreversible capacity [9]. Fig. 7a and b show that the shape of the Nyquist plot for kinetic Li insertion–extraction at the open-circuit potential (OCP, point A in the Figs.) was a depressed semicircle in the high frequency region and a sloping line of variable gradient in the low frequency region. On Li intercalation, the dimensions of the depressed semicircles decrease, and a new depressed semicircle appears in the middle frequency region below 0.5 V (point D). Fig. 6c shows that the overall structure of the Nyquist plot for intrinsic impedance consists of a depressed semicircle with a reactance line. The resistance determined from the intersection of the high-frequency line with the real axis is the electronic resistance of the graphite, and the small semicircle corresponds to the particle-to-current collector contact impedance [9]. The high-frequency **inductive** reactance in the EIS used for intrinsic resistance measurement is an instrumental artifact which disappears when the measured resistance is high [9]. The contact resistance in the electrode decreases with Li content due to the volume expansion on lithiation. On initial Li insertion into JM 287, electronic resistance initially decreases as the potential falls from the OCP to 0.94 V (point B in Fig. 6c), then it begins to increase, reaching a maximum value at 0.63 V in the potential region where the SEI film is first formed. The initial decrease in the graphite electronic resistance may be attributed to removing impurities from the graphite surface, whereas the following increase may be due to co-insertion of electrolyte into the graphite during the process of SEI formation. Below 0.6 V (point C) the electronic resistance of the graphite again decreased because of the high conductivity of lithiated graphite [9]. The use of the special EIS proto-

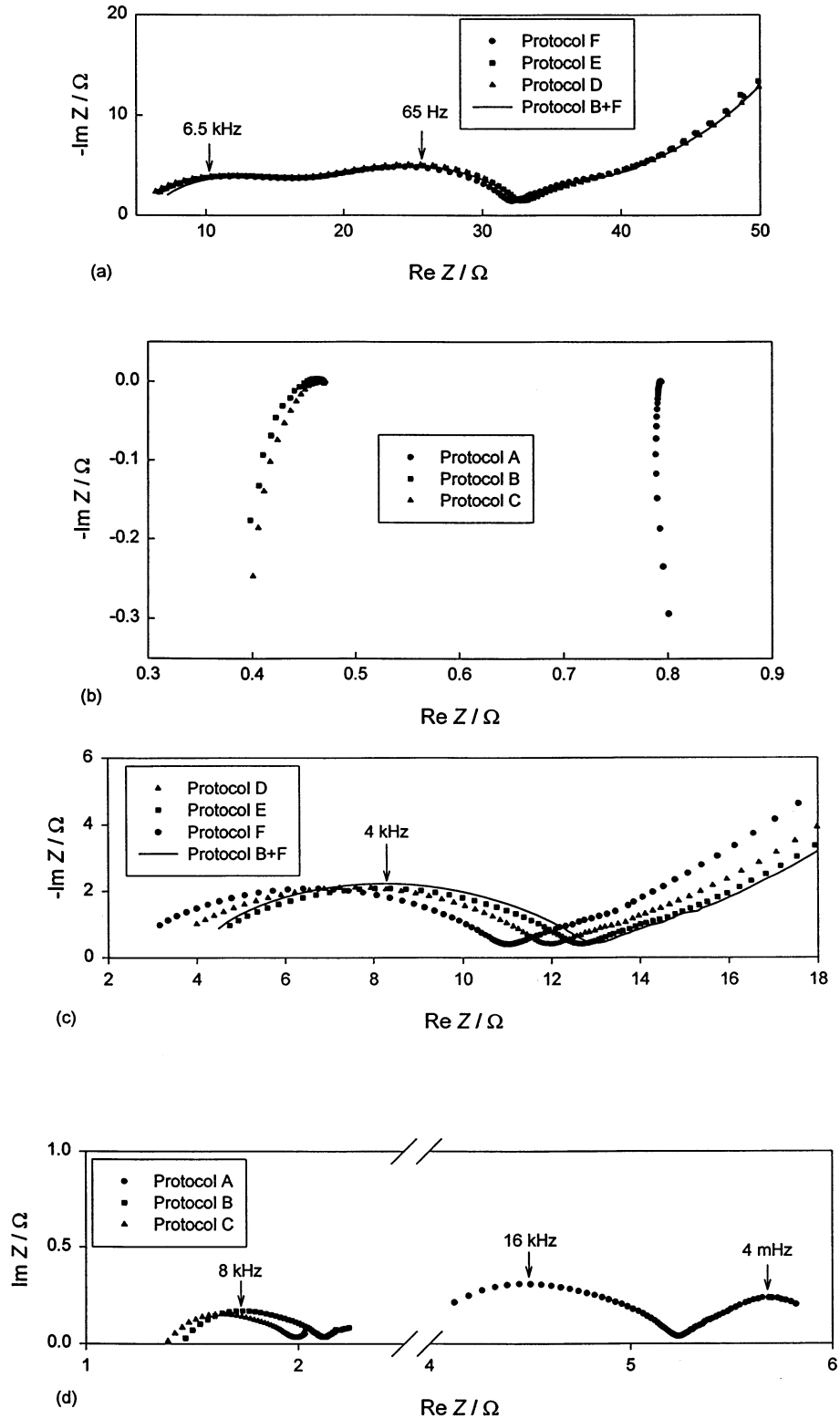

Fig. 5. Nyquist plots for kinetics of lithium insertion–extraction (a and c) and intrinsic impedance (b and d) of JM 287 graphite in 1.0 M $LiPF_6$, PC:EC:DMC (1:1:3) solution at 80 mV using different Solatron electrochemical interface terminal-electrode connections. (a) and (b) after 12 galvanostatic (5 mA/g) charge–discharge cycles, (c) and (d) after five potentiostic charge–discharge cycles at 1.5 and 0 V, following by 40 galvanostatic (5 mA/g) charge–discharge cycles. Each potentiostic charge–discharge step was initiated only when the current became less than 1 μA.

cols in the previous section shows that the first depressed semicircle consisted of a combination of contact and SEI film impedance. However, the large semicircle in Fig. 7b at the OCP cannot be explained in this manner since the SEI film had not yet formed and the contact resistance was very small (Fig. 7c) at the OCP (point A). Furthermore, the dimensions of the first semicircle in the high frequency region decrease with the amount of Li inserted in the potential region where SEI film formation occurs (0.9–0.2 V). The only explanation accounting for these observations is that the second semicircle is related to that for the charge-transfer reaction, which initially relates to the impedance corresponding to the first semicircle at the OCP. On insertion of lithium, the first semicircle moves to the high-frequency region, while the second moves to the low-frequency region, leading to complete separation of the two at low potentials. This explanation is verified by the variation of the apparent characteristic frequency as a function of the amount of lithium inserted (Fig. 6), and by numerical analysis of EIS in Fig. 7a given in a later section. During further charge–discharge cycling, the apparent characteristic frequencies of the two depressed semicircles were relatively stable, and both semicircles were affected by SEI film formation.

Analysis of EIS data has the possibility of giving multiple interpretations of the reaction mechanism. However, if the data are analyzed logically, it is possible to minimize uncertainties. The logic used in this and previous work was to propose an impedance model based on experimental results obtained in this laboratory and elsewhere [6,7,10,12,13]. The common feature of the EIS for Li insertion–extraction to and from graphite is the presence of two depressed semicircles, with a Warburg-like line corresponding to the finite diffusion of lithium in graphite particles. The results show that the first depressed semicircle is largely due to the SEI film impedance, increased somewhat by the contact resistance within the electrode. An equivalent-circuit model consisting of four or five parallel RC circuits was used to simulate the SEI film [6,10]. This describes a multilayer SEI film with a compact structure in the innermost layer and a porous structure in the

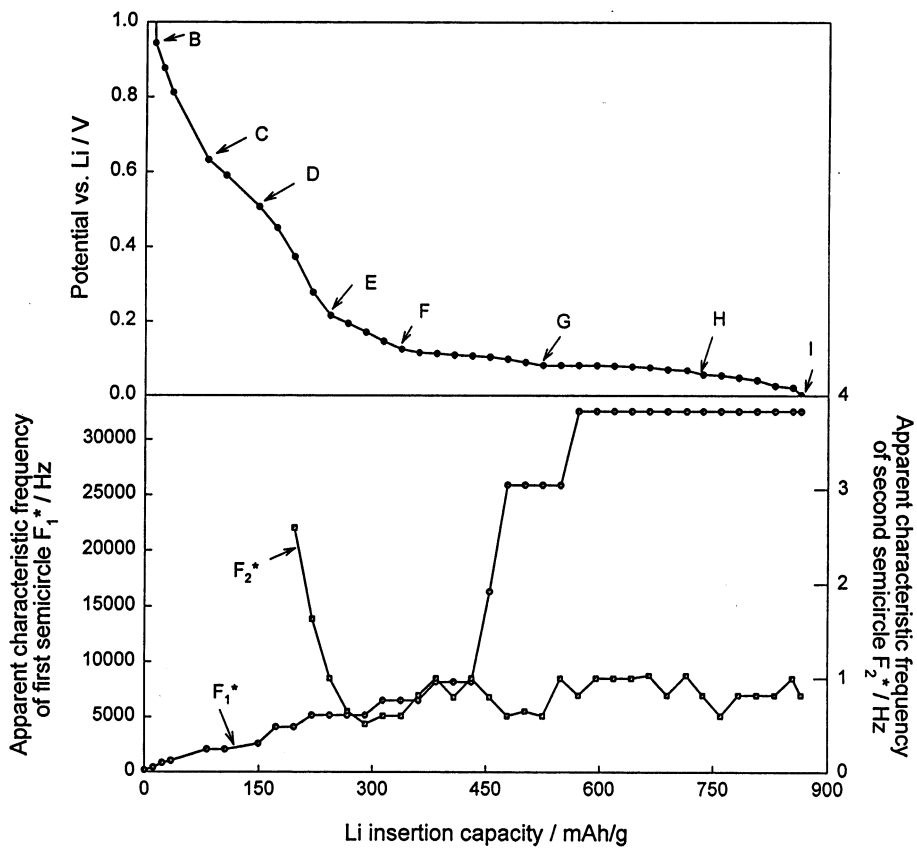

Fig. 6. Potential and apparent characteristic frequency of two semicircles dependence of JM 287 anode as a function of charge capacity during initial charging at 25°C. The potentials were measured at the end of current pulses (6.5 mA/g for 4 h). After 10 h relaxation time at each point, EIS measurements for intrinsic and reaction resistance were obtained.

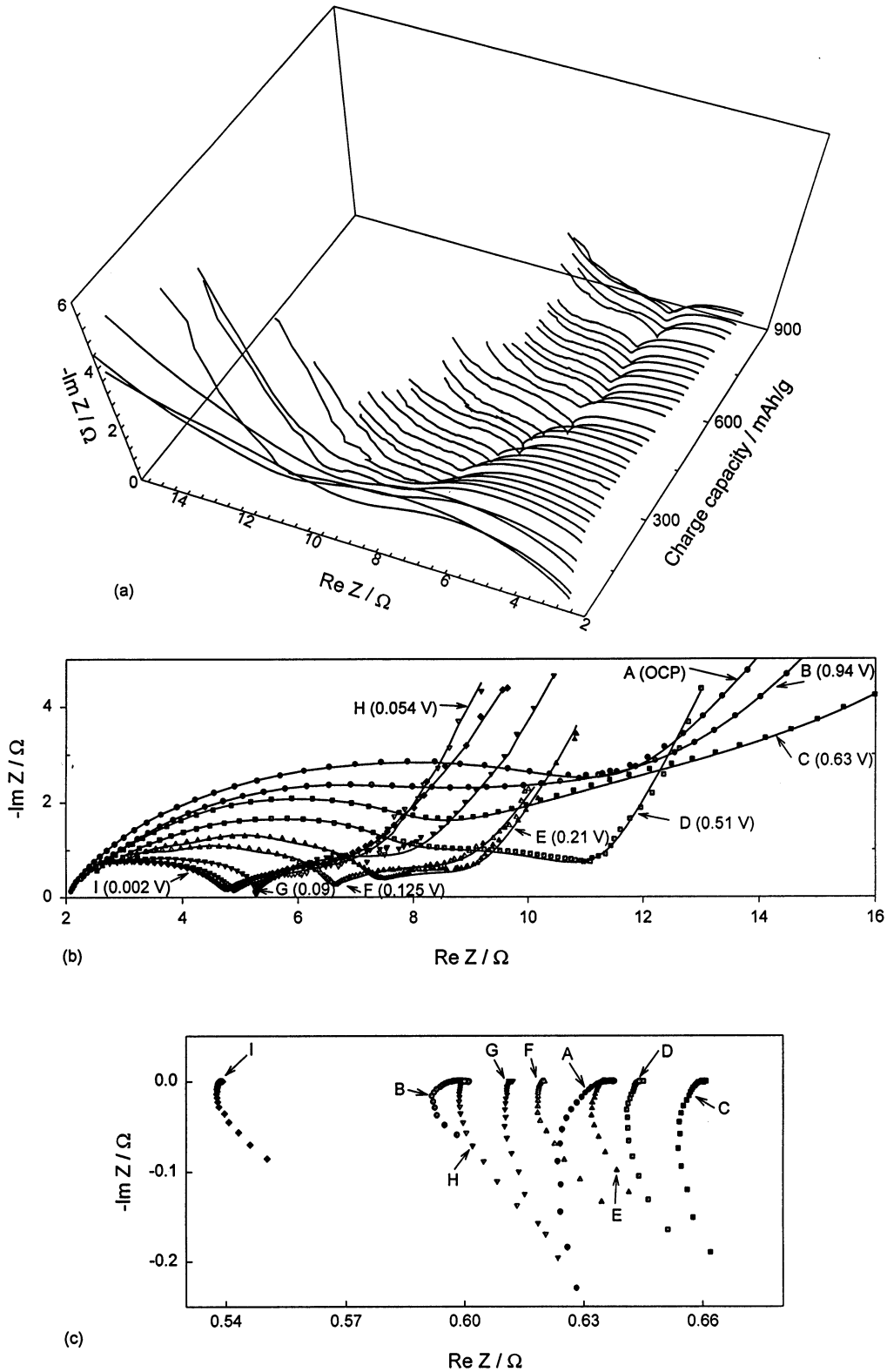

Fig. 7. Nyquist plots for (a) and (b), reaction kinetics and (c), intrinsic impedance measured at different degrees of intercalation levels during initial Li insertion into a JM 287 anode at 25°C. (b) is the selected EIS from (a) as specified in Fig. 6. (c) is the selected intrinsic impedance as specified in Fig. 6. EIS Protocol **D** was used for lithium insertion–extraction kinetic measurement and Protocol **A** was used for intrinsic impedance measurement. The solid lines in (b) are the fitting results from the equivalent circuit

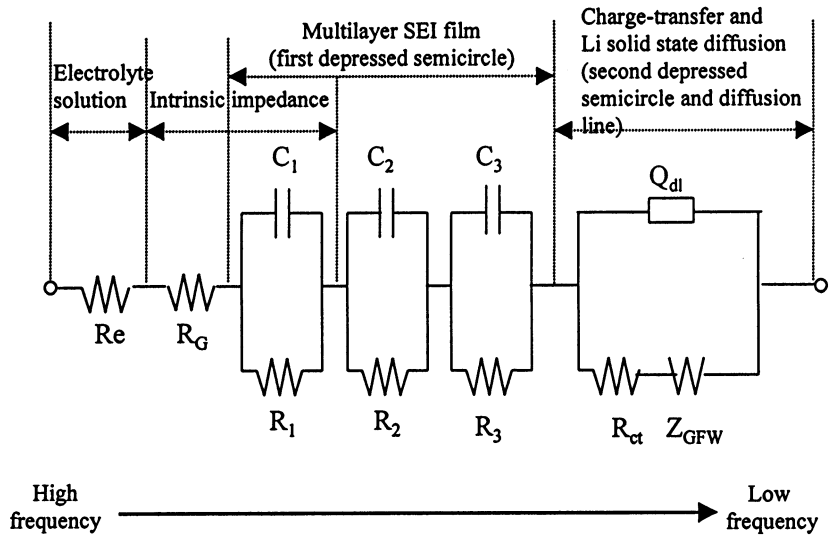

Fig. 8. Equivalent circuit used for analysis of impedance spectra for initial Li intercalation into JM 287 graphite at 25°C and 65°C. R_e and R_G: ionic electrolyte and electronic graphite resistances. R_1–R_3: resistances for Li^+ migration through each of the three model SEI film layers (R_1 includes the SEI–graphite contact resistance). C_1–C_3: the corresponding SEI layer capacitances (C_1 includes the contact impedance). R_{ct} and Q_{dl}: charge-transfer resistance and constant phase element related to double-layer capacitance. Z_{GFW}: generalized finite Warburg impedance for solid-state Li diffusion in the bulk electrode.

outer layer. This will result in a number of fitting parameters, which may give multiple results. Peled et al. suggested the use of a model consisting of three different layers (three parallel RC circuits) to fit their EIS data [12]. A series of three parallel RC circuits was therefore used in this work to attempt to fit the first depressed semicircle. An individual parallel RC to simulate contact impedance was not used, due to its very small value ($< 0.01\ \Omega$ in Fig. 7c), which increases the impedance of SEI layer to a small extent only in the highest frequency range. Since the intrinsic impedance is in series with the reaction kinetic impedance, any change in the electronic resistance of the graphite will affect the electrolyte resistance measured from the intersection of the high-frequency line with the real axis. The second semicircle in Fig. 7a and b is not a real parallel RC circuit, but a depressed semicircle. Hence, a constant phase element (CPE, symbol Q_{dl}) is used for simulating the EIS for the charge-transfer reaction [13]. The expression for the admittance response of the Q_{dl} is:

$$1/Q_{dl} = C_{dl}\omega^n \cos(n\pi/2) + jC_{dl}\omega^n \sin(n\pi/2) \quad (1)$$

where ω is the angular frequency, $j = \sqrt{-1}$, C_{dl} is considered to be a pseudo double layer capacitance (pseudo-C_{dl}) where n is not equal to 1, but lies between 0 and 1.

The generalized finite Warburg element (GFW) was used to fit the lithium diffusion in graphit and may be expressed as follows:

$$Z_{GFW} = R\ \tanh[(j\omega T)^\theta]/(j\omega T)^\theta \quad (2)$$

where T is a time constant, R is resistance, and θ is an exponent. Fig. 8 depicts the equivalent circuit used to fit the impedance of the first Li insertion–extraction cycle of JM 287 graphite. A step by step, double-check fitting method was used in the numerical analysis of the impedance spectra during the first charge process. In this, the fitted parameter values in the previous step (with lower lithium content) were used as initial values for the following step, and then the fitted parameters in the following step were used as initial values to fit the spectra of the previous step. The two processes were repeated until the values of the parameters fitted became the same by fitting in both the forward and backward directions. The relative standard deviation for all parameters fitted did not exceed 15%. Some simulated impedance spectra for the first charge at room temperature are compared with experiment in Fig. 7b. The proposed model describes the experimental data satisfactorily for different degrees of intercalation.

The parameters obtained from fitting the room-temperature data for the first charge process are shown in Fig. 9. The resistances of all three SEI layers have a similar value around 0–2.5 Ω. However, the capacitances of the three SEI layers, which are inversely proportional to their thicknesses, are quite different. The small capacitance (C_1) may be attributed to that of the compact inner layer (in contact with graphite) and the larger capacitance (C_3) to that of the outer porous layer (in contact with the electrolytic solution), because

the latter has the larger surface area [6]. The very small value of the three resistances (R_1–R_3) and the larger values of the three capacitances (C_1–C_3) at the OCP indicate that the semicircle represents the impedance of the charge-transfer reaction. On charging, the capacitances of the three SEI layers rapidly decrease on going from the OCP to 0.8 V. The rate of decrease becomes slower during further charge to 0.6 V. The changes in

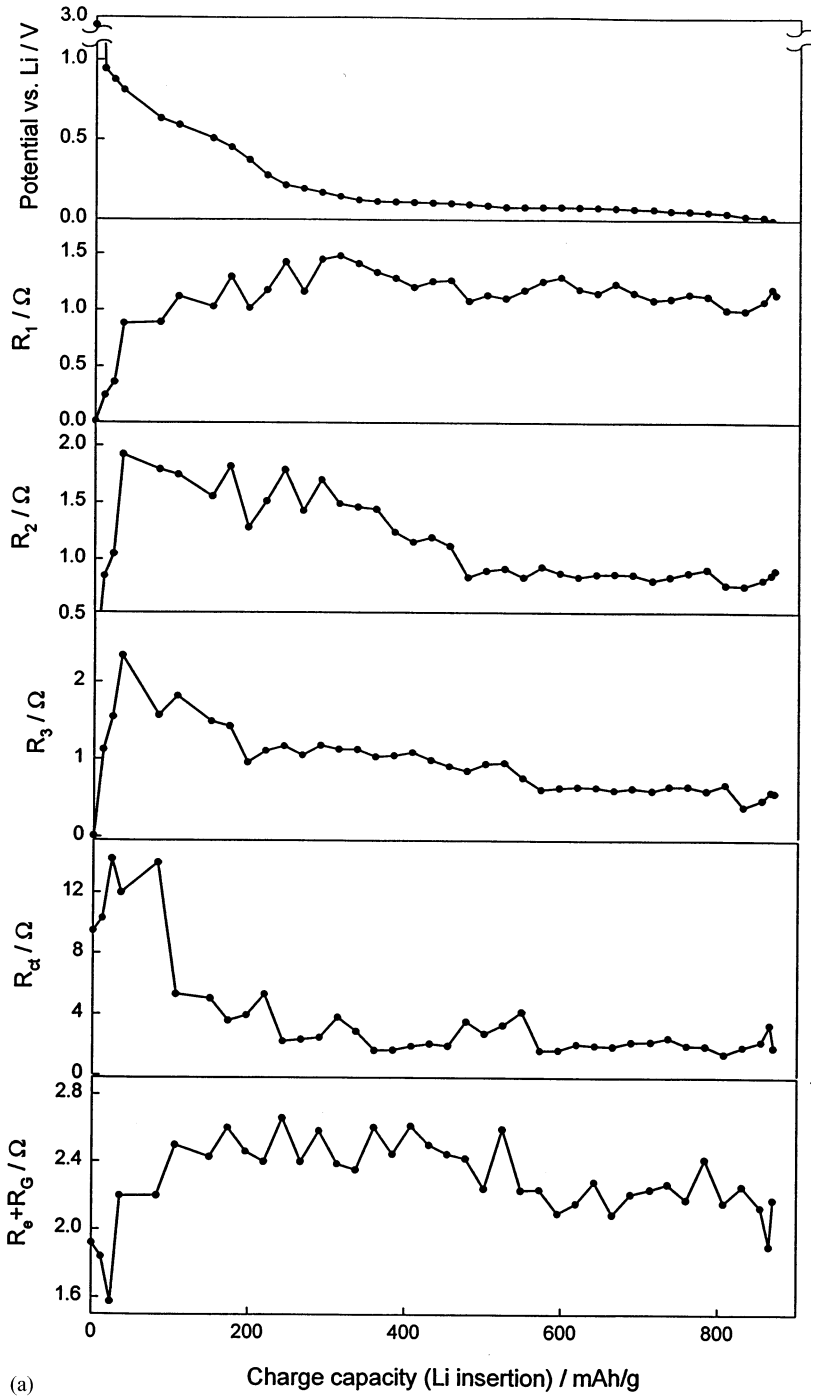

Fig. 9. Parameter values obtained from fitting the experimental impedance spectra of JM 287 graphite during initial charge (Li insertion) at 25°C. The double-layer capacitance C_{dl} is considered to be a pseudo-C_{dl} because the parameter n is around 0.5, not 1.

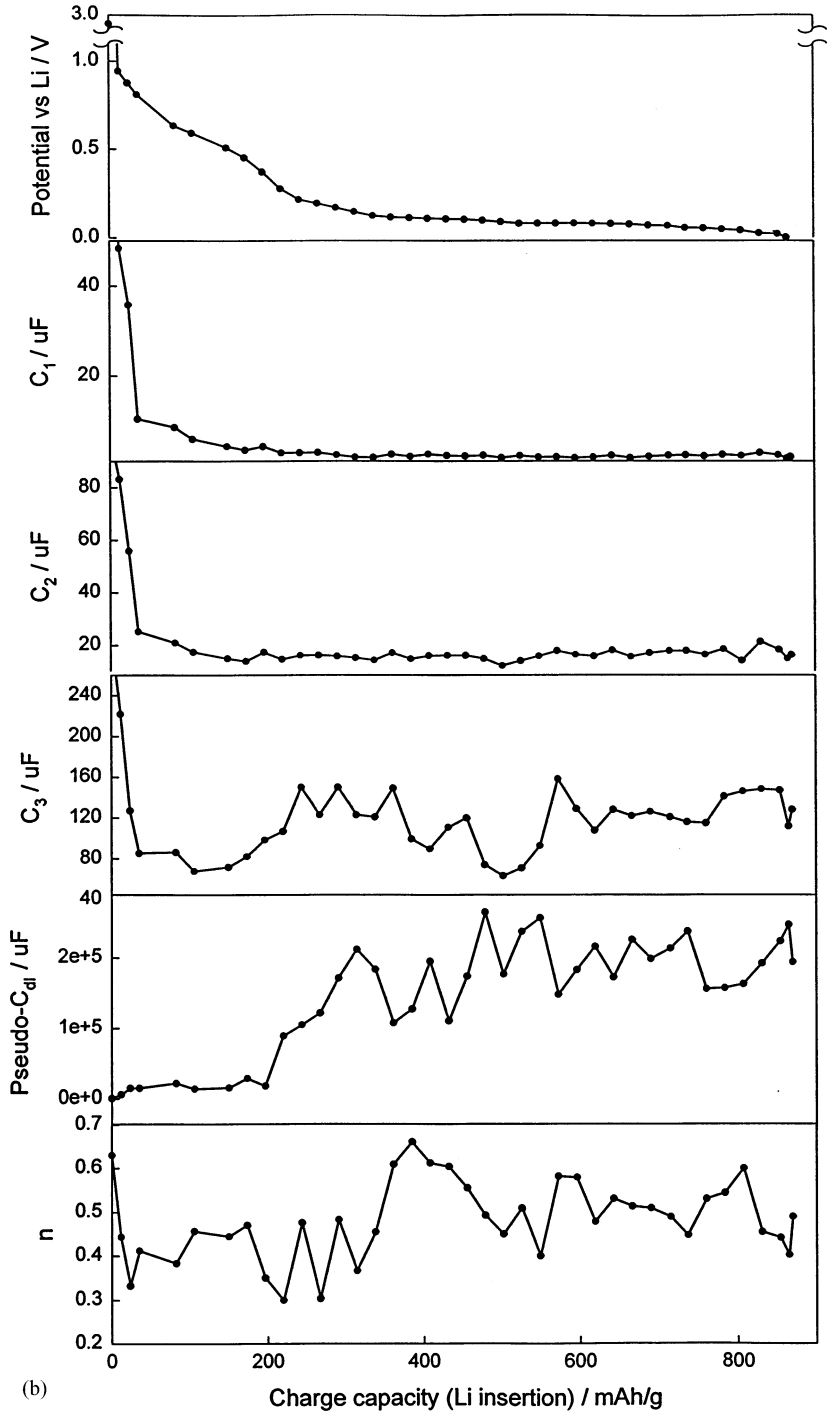

Fig. 9. (*Continued*).

the capacitance values indicate that the SEI film forms between OCP and 0.8 V, and then further growth occurs during charge to 0.6 V. SEI formation can also be inferred from the increase in resistances R_1–R_3 in the potential range from OCP to 0.8 V. On further charging, R_1 continues to increase, but R_2 and R_3 begin to decrease. The decrease in R_2 and R_3 may be associated with electrolyte co-insertion into graphite [15],

giving a volume expansion resulting in a decrease in the resistivity and in the thickness of the less compact middle and outer layers of the SEI film. Compression resulting from electrolyte co-insertion in the potential range 0.6–0.2 V decreases the thickness of the outer porous layer, giving an increase in C_3. When lithium insertion begins at less than 0.2V, the thicknesses of the three layers become relatively stable, with some scatter for C_3. The influence of the contact impedance of graphite on the SEI impedance is very small because the contact resistance change during first Li insertion process ($< 0.01\ \Omega$ in Fig. 6c) is much smaller than that for R_1, which lies between 0.2 and 1.5 Ω. The above analysis of the formation and growth of the SEI film on graphite using EIS is in agreement with results observed by atomic force microscopy [16] and SEM [17].

SEI film formation also affects the charge transfer reaction at the graphite-SEI film interface. In Fig. 9 the double layer capacitance C_{dl} is considered to be a pseudo capacitance because n is not equal to 1. During the first charge, the pseudo-C_{dl} increases somewhat in the SEI film formation potential range (0.94–0.2 V). Then increases is more rapidly at lithium insertion potentials around 0.2 V, and then remains essentially stable (with some scattered points) on further Li insertion. The charge transfer resistance initially increases during SEI formation, and then decreases from 0.6 to 0.2 V, stabilizing at below 0.2 V. The small increase in pseudo-C_{dl} but rapid decreases in R_{ct} as potential goes from 0.6 to 0.2 V may be explained by an increase in the contact area between graphite and the SEI film as a result of electrolyte co-intercalation into graphite**.** Electrolyte co-intercalation begins at the edge of the graphite planes [15], opening them and increasing the contact area between the graphite and the SEI film.

The results shown in Fig. 9 also confirm that the decrease in capacitance of each SEI layer and the increase in the pseudo-C_{dl} value during initial lithium insertion into graphite are associated with a depressed SEI semicircle. The latter moves to the high frequency region, while the depressed charge-transfer semicircle moves to the low frequency region. Both finally become separated below 0.5 V.

Lithium insertion into graphite decreases the graphite electronic (R_G) resistance, but by-product contamination of the electrolyte due to its reduction during SEI formation [14] will increase the contact resistance (R_e). This results in a change in $R_e + R_G$ during SEI formation and in the Li insertion region.

3.5. EIS measurements on JM 287 anodes during initial charging at 65°C

Another identical JM 287 electrode was pulse charged at 65°C. Fig. 9 shows that the measured potential and the apparent characteristic frequency at the end of each charge current pulse (4 h, 6.5 mA/g) at 65°C as a function of charge capacity. After 10 h relaxation time for each current pulse, EIS Protocols **A** and **C** were used for lithium insertion–extraction kinetic and intrinsic impedance measurement, respectively. Fig. 11a shows the reaction kinetics impedance measurement at different Li content. Fig. 11b–e show selected Nyquist plots to determine the reaction kinetics and intrinsic resistances at the Li insertion levels specified in Fig. 10. Experimental data are given as dots, and fitted results are solid lines. The reaction kinetics and intrinsic impedance after 1 day on stand at 25°C (point B in Fig. 11b) were almost the same as those at the OCP in Fig. 7b (point A), confirming that the two JM 287 electrodes were identical.

To investigate the influence of SEI film formation at 25°C on behavior at 65°C, the JM 287 electrode was first pulsed charge at 65°C to 350 mAh/g, and then was cooled to 25°C. It was then further charged at this temperature to 90 mV versus Li/Li^+, where the SEI film was completely formed. The cell was then heated to 65°C, and further charged with same pulsed current. The negative values in Figs. 10 and 11a correspond to the relaxation time imposed after the electrode was assembled in the glove box at 25°C. Over 1 day of relaxation at 25°C, the potential of the JM 287 potential gradually increased from 2.8 to 2.95 V (Fig. 10). However, the apparent characteristic frequency was stable at 516 Hz, and the reaction resistance increased slightly (Fig. 11b). The intrinsic resistance decreased, with a change in its impedance plot from two semicircles to one small semicircle (Fig. 11c). The two intrinsic impedance semicircles are associated with particle-to-current collector and particle-to-particle contact impedances [9]. The decrease in intrinsic resistance with time may result from electrolyte impregnation into the electrode porosity, and perhaps to reaction with impurities. When the electrode was charged with a pulsed current at 65°C, the potential rapidly decreased, then stabilized at 1.1 V (Fig. 10). The apparent characteristic frequency of the first semicircle in Fig. 10 increased during the change in potential from 2.95 to 1.1 V, and then began to decrease on further charging at 1.1 V. This behavior is quite different from that at 25°C (Fig. 6). The existence of a potential plateau at 1.1 V indicates that no passive SEI film formed during this period. The passive SEI film formed after charging at 25°C, covered now by new film, was not useful in initiating passive SEI film formation during further charging at 65°C. This is clear because the potential was still at ca. 1.1 V after the sample was charged again at 65°C. However, the film did inhibit electrolyte co-insertion into graphite, as the numerical analysis in the following section shows. This did improve the cycling capacity stability of JM 287 at 65°C, as Fig. 3 shows. The reaction impedance during charge at 65°C (Fig.

11d) shows an increase in resistance of the semicircles during the initial charge at 65°C, followed by a small decrease during the second charge. The intrinsic resistance of the graphite showed an increase during initial charge cycles at 65°C, following by a decrease and then increase again during the second charge (Fig. 11e). The increase in intrinsic and reaction resistances during the first charge at 65°C may be related to electrolyte co-insertion into graphite. The decrease in the same resistances during the second charge may be explained by the conversion of SEI film from a metastable to a stable phase [8]. A continued increase in intrinsic resistance was observed during charge at 25°C after an initial charge of 350 mAh/g at 65°C, indicating different behavior from that shown in Fig. 7c.

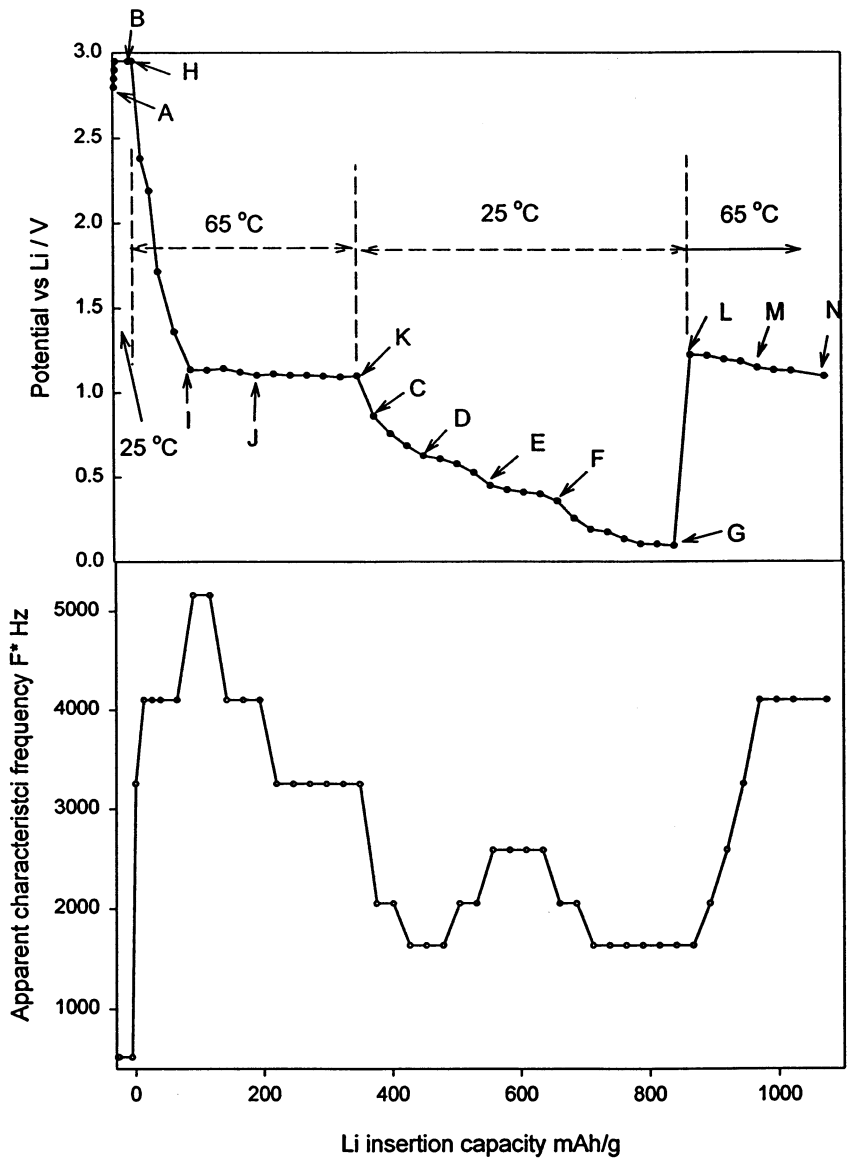

Fig. 10. Potential and apparent characteristic frequency of semicircle dependence of a JM 287 anode on charging capacity during the initial charge process at 65°C. The potentials were measured at the end of current pulses (6.5 mA/g for 4 h). After 10 h relaxation time at each point, EIS measurements for intrinsic and reaction resistance were obtained. After pulsed charging at 65°C to 350 mAh/g, the electrode was cooled to 25°C and further charged to 90 mV, at which the SEI film was completely formed. The graphite was then heated to 65°C and further charged at the same pulse current. The negative time corresponds to the time the graphite electrode was assembled in the glove box at 25°C.

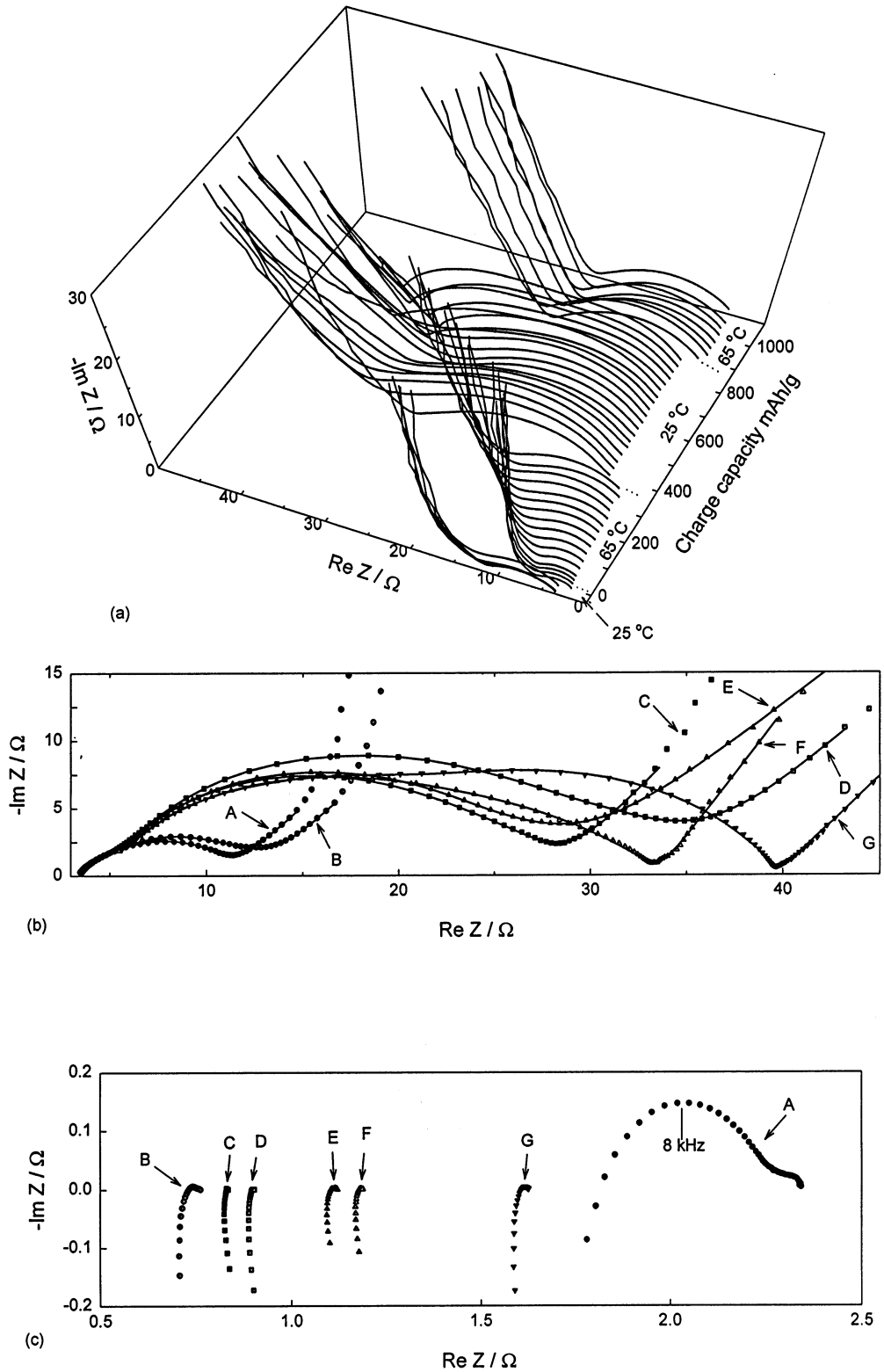

Fig. 11. Nyquist plots for (a), (b), and (d) reaction kinetics and (c) and (e) intrinsic impedance measured at different degrees of intercalation levels during initial Li insertion into a JM 287 anode at 25°C and 65°C. (b) and (d) are the selected EIS from (a), which is specified in Fig. 10. (c) and (e) are the selected intrinsic impedance specified in Fig. 10. EIS Protocol **D** was used for measurement of lithium insertion–extraction kinetics and Protocol **A** was used for intrinsic impedance measurement. The solid lines in (b) are the fitting results using the equivalent circuit of Fig. 8.

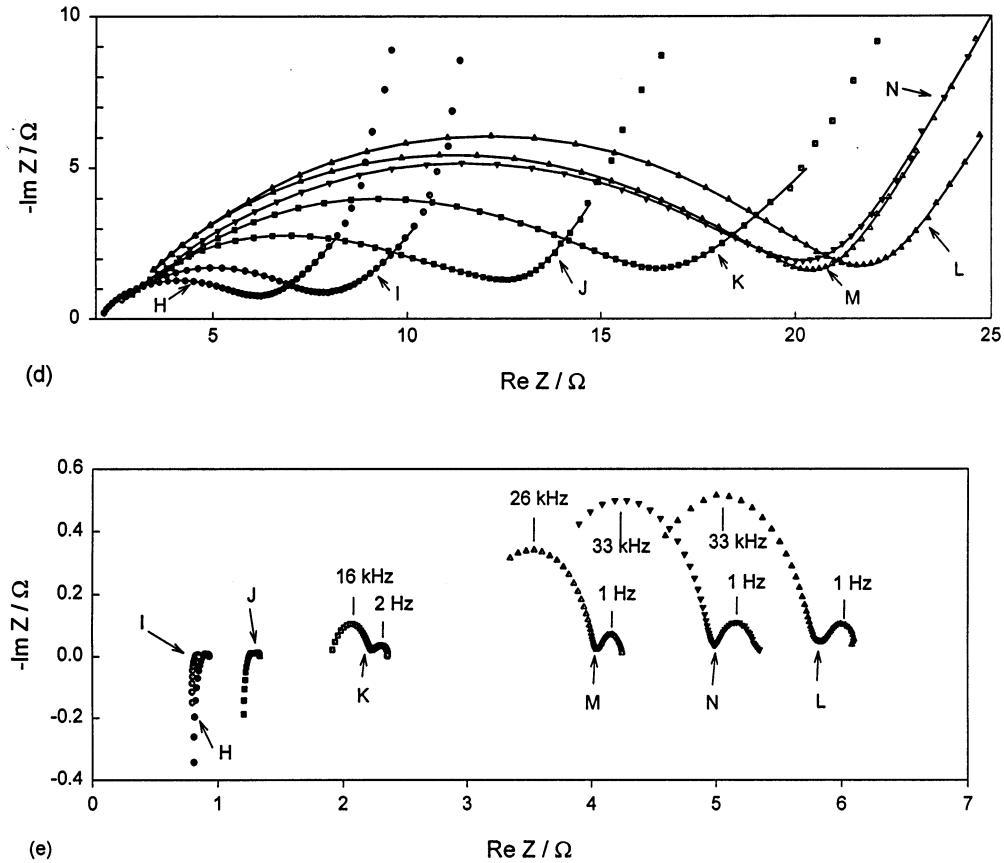

Fig. 11. (*Continued*).

To gain insight into the changes in JM 287 impedance in Fig. 11a, numerical analysis were performed using the equivalent circuit in Fig. 8. The change of parameters as determined from analysis of impedance spectra in Fig. 10a is shown in Fig. 12. During the first charge from the OCP to 1.1 V at 65°C, the three SEI capacitances rapidly decreased, but the corresponding resistances were almost constant except for an initial increase from the OCP to 2.38 V. This indicates that an SEI film with a very thin inner layer and a porous outer layer was formed on the graphite surface. As in charging at 25°C, the pseudo-C_{dl} increased in this potential range. Further charging at the 1.1 V plateau initially produced a further decrease in the three SEI capacitances, followed by an increase, with a continuous decrease in the pseudo-C_{dl} throughout the potential region. This change can be explained by co-insertion of electrolyte. The capacitance of each layer SEI can be approximately calculated using the following equation:

$$C_i = \varepsilon\varepsilon_o A/d_i \quad (3)$$

where d_i is the thickness of the ith layer of the SEI film, ε_o is the vacuum permittivity, ε is the general permittivity, and A is the electrode area.

The increase in capacitance of the innermost layer may be explained by the increase in SEI film thickness, along with further electrolyte co-insertion into graphite. The latter exfoliates the graphite planes, giving graphite–SEI film mixtures or graphite dust [10] with porous inner layer structures of increased area and capacitance. As at 25°C (Fig. 9), C_3 will also increase in the potential range for electrolyte co-intercalation at 65°C due to the resulting volume expansion. Initial electrolyte co-insertion into the graphite planes at 65°C forms a zigzag interface between the SEI film and graphite [15] (as at 25°C), resulting in an increase in the contact area between the SEI and graphite. This leads to an initial increase in C_{dl} but a decrease in R_{ct}. In contrast, further electrolyte co-insertion into the graphite planes at 65°C exfoliates the graphite layers, giving a reduced contact area between the active bulk graphite and SEI, which results in the increase in R_{ct} and the associated decrease in pseudo-C_{dl}, as Fig. 12 shows. Co-insertion of electrolyte also results in a large

increase in intrinsic resistance, as is shown at points I, J, and K in Fig. 11e. Other evidence for electrolyte co-intercalation is that the discharge capacity of the graphite on its first discharge under these conditions is only about 80 mAh/g, compared to 300 mAh/g for graphite charged at 25°C. The low discharge capacity is not due to mechanical breakdown of the graphite electrode because the contact resistance is still about 6 Ω during the first charge (Fig. 11e). Some graphite powder was found at the bottom of the cell after the first cycle, which may result from the co-intercalation of electrolyte into graphite. The increase in the characteristic frequency of the charge-transfer process is associated with in an decrease in pseudo-C_{dl}, which results in the mingling of the charge transfer and SEI film semicircles, again very different behavior from that at 25°C. In addition, the amount of co-insertion of electrolyte is small at 25°C, giving a small reduction in C_3, associated with decreasing resistances in the SEI film layers and in R_{ct} and increasing pseudo-C_{dl} in the co-insertion potential region.

The passive SEI layer at 25°C was considered to be completely formed after charging to a potential of 90 mV. The values R_2, R_3 and R_{ct} at 65°C were at least five times higher than at 25°C (Fig. 9). Thus, the layer produced by pre-charging at 65°C to 350 mAh/g, followed by charging at 25°C was at least five times thicker than that formed at 25°C. A comparison of the C_3 values at 90 mV in Figs. 9 and 12 shows that the thickness of porous layer formed after pre-charging at

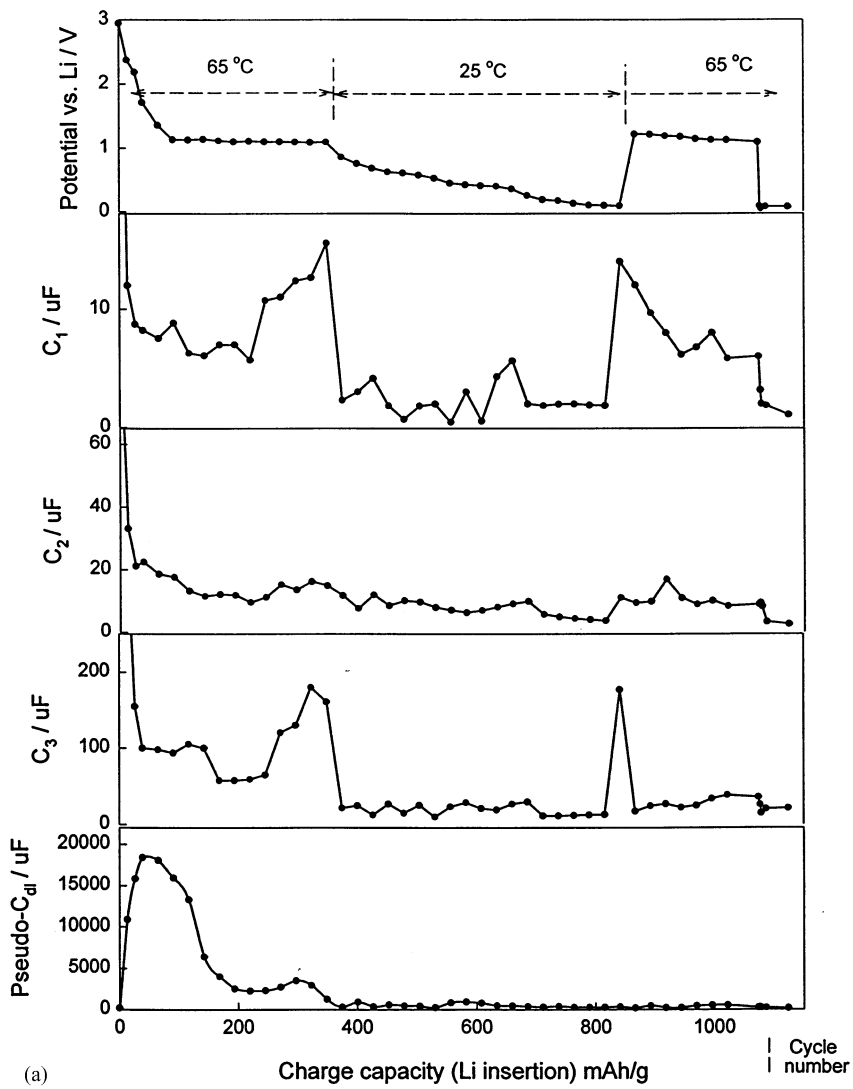

Fig. 12. Parameter values obtained from fitting the experimental impedance spectra in Fig. 11a during the initial charge at 25°C and 65°C using the equivalent circuit of Fig. 8 and the procedure in Fig. 7.

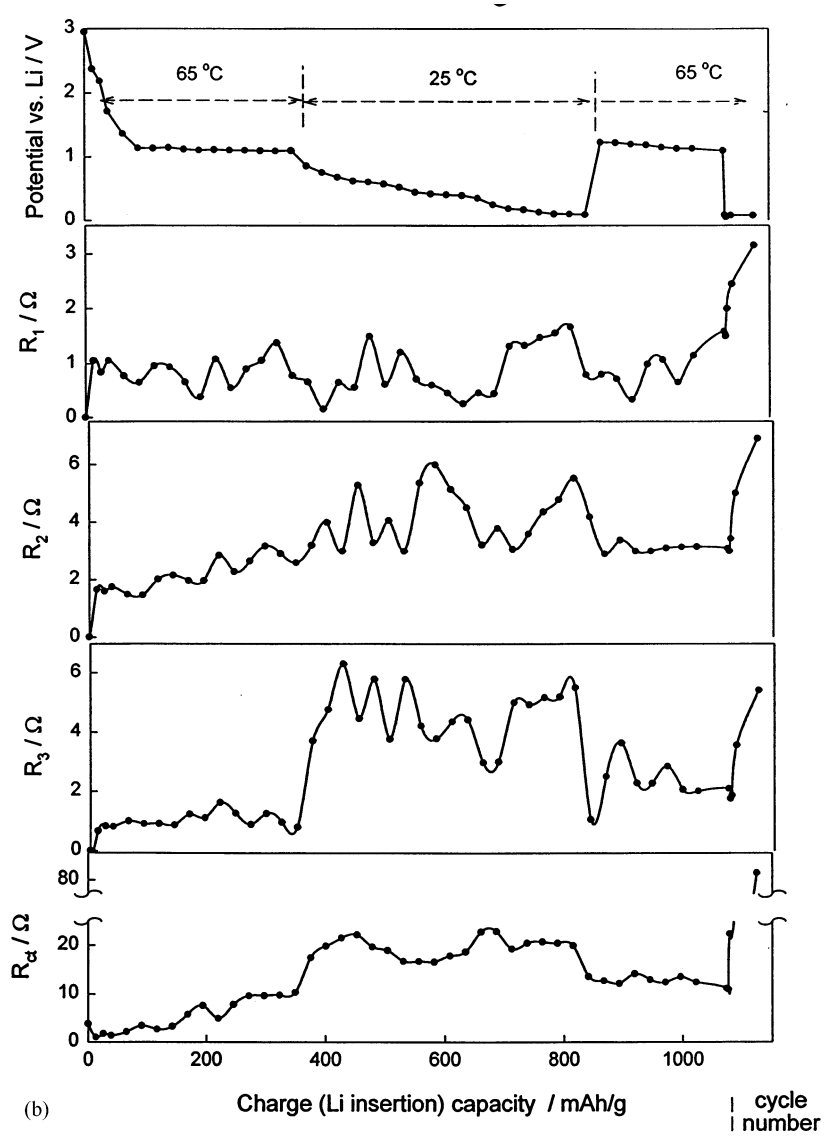

Fig. 12. (*Continued*).

65°C was three times greater than that produced at 25°C. The fact that charging at 25°C following initial charging at 65°C limited electrolyte co-insertion during a following charge at 65°C is shown by the decrease in C_1, with $R_{ct,}$, C_3, and the intrinsic resistance remaining stable during the second charge cycle at 65°C (Fig. 11e).

A large decrease in C_1–C_3 but an increase in R_1–R_3 and R_{ct}, which resulted from the growth of SEI film, were observed during the following 30 charge–discharge cycles. The unstable SEI film also increased the intrinsic resistance, leading to a separation of graphite particles.

The intrinsic impedance was not included in the equivalent circuit in Fig. 8 for the reasons already discussed. The contact resistances during the first charge at 65°C and after charging at 25°C were within 0.5 Ω (Fig. 11c and e), and only 25% of this value (< 0.13 Ω) will affect the reaction resistance as measured by Protocol **D** [8]. The total resistance of the first SEI film semicircle was higher than 4 Ω (Fig. 12). Hence, the relative error in the analysis of a SEI film using the equivalent circuit in Fig. 8 was smaller than 4%, increasing to 10% during the second charge cycle at 65°C.

Finally, the thermal stability of the electrolyte at 65°C was monitored in situ by measuring the impedance of a floating Pd wire electrode. Selected Nyquist plots for this electrode in the high frequency

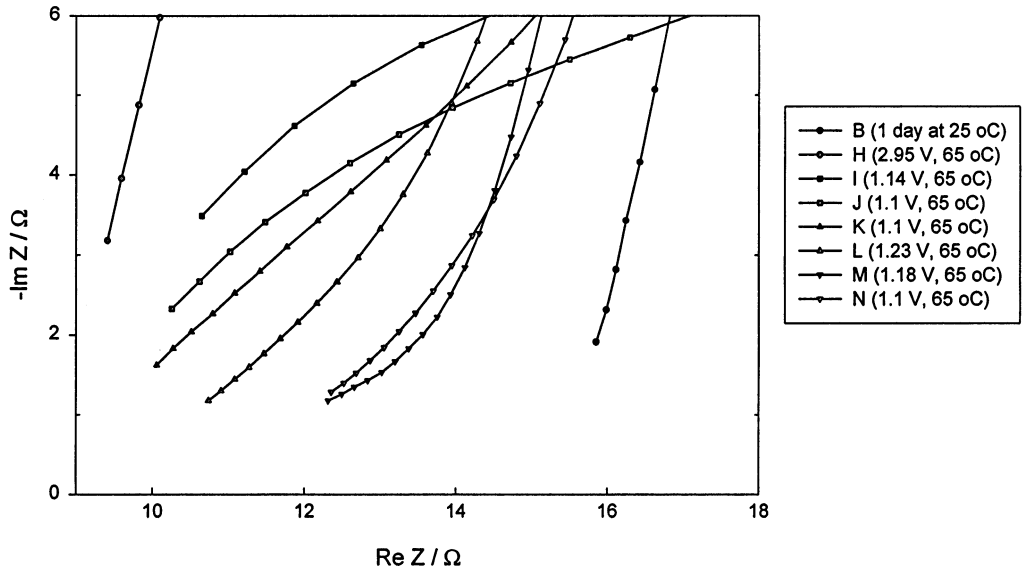

Fig. 13. Selected Nyquist plots for a floating palladium wire electrode in the experimental electrolyte at the potential specified in Fig. 10.

range at potentials specified in Fig. 10 are shown in Fig. 13. The palladium surface area exposed to the electrolyte remains constant, since no SEI film is present, and the distance between the Pd electrode and the Li reference electrode is constant, so the intersection of the high-frequency lines with the real axis indicate the electrolyte conductivity. In Fig. 13, the small decrease in conductivity during Li insertion at 65°C indicates that the electrolyte is relatively stable at this temperature. The increase in conductivity from points B to H results from the change in temperature from 65°C to 25°C.

4. Conclusions

Special EIS protocols have been applied to PVDF-bonded JM 287 graphite electrodes sandwiched between nickel current collectors to investigate the formation of the interface (SEI) film during initial lithium insertion at ambient temperature and at 65°C. The EIS protocol to measure reaction kinetic impedance and intrinsic (i.e. physical) impedance show that both are in series. Numerical analysis using an equivalent circuit indicated that the EIS semicircle at the open-circle potential corresponds largely to the impedance of the charge-transfer reaction. The capacitances of the SEI film layers decrease but the pseudo-double-layer capacitance increases during SEI formation on initial charging (Li insertion) at 25°C. This results in a movement of the SEI film semicircles to the high frequency region, while the charge-transfer semicircle moves to lower frequencies, which results in the appearance of two separated depressed semicircles at low potentials. The formation of a porous SEI film together with electrolyte co-insertion into graphite during the first charge at 65°C result in high intrinsic and charge transfer resistances, giving a short cycle life. Pre-charging at 25°C improves the cycle life of the graphite electrodes studied at 65°C since the SEI film formed at 25°C inhibits co-insertion of the electrolyte graphite during subsequent cycling at 65°C.

Acknowledgements

We gratefully acknowledge NASA-Glenn Research Center, Cleveland OH, for support of this work.

References

[1] D. Aurbrach, Y. Ein-Eli, O. Chusid, Y. Carmeli, M. Babai, H. Yamin, J. Electrochem. Soc. 141 (1994) 603.
[2] A.M. Anderson, K. Edstrom, N. Rao, A. Wendsjo, J. Power Sources 81-82 (1999) 186.
[3] M.N. Richard, J.R. Dahn, J. Electrochem. Soc. 146 (1999) 3596.
[4] T. Zheng, A.S. Gozdz, G.G. Amatucci, J. Electrochem. Soc. 146 (1999) 4014.
[5] E. Barsoukov, J.H. Kim, J.H. Kim, C.O. Yoon, H. Lee, J. Electrochem. Soc. 145 (1998) 2711.
[6] C.R. Yang, J.Y. Song, Y.Y. Wang, C.C. Wan, J. Appl. Electrochem. 30 (2000) 29.

[7] Y.C. Chang, H.J. Sohn, J. Electrochem. Soc. 147 (2000) 50.
[8] C.S. Wang, A.J. Appleby, F.E. Little, J. Electroanal. Chem. 497 (2001) 33.
[9] C.S. Wang, I. Kakwan, A.J. Appleby, F.E. Little, J. Electroanal. Chem. 489 (2000) 55.
[10] D. Aurbach, B. Markovsky, I. Weissman, E. Levi, Y. Ein-Eli, Electrochim. Acta 45 (1999) 67.
[11] M. Yoshio, H. Wang, K. Fukuda, Y. Hara, Y. Adachi, J. Electrochem. Soc. 147 (2000) 1245.
[12] E. Peled, D. Golodnitsky, G. Ardel, J. Electrochem. Soc. 144 (1997) L208.
[13] T. Piao, S.M. Park, C.H. Doh, S.I. Moon, J. Electrochem. Soc. 146 (1999) 2794.
[14] D. Aurbach, A. Zaban, J. Electroanal. Chem. 348 (1993) 155.
[15] M. Winter, P. Novak, A. Monnier, J. Electrochem. Soc. 145 (1998) 428.
[16] A.C. Chu, J.Y. Josefowicz, G.C. Farrington, J. Electrochem. Soc. 4146 (1997) 428.
[17] K. Zaghib, K. Tatsumi, Y. Sawada, S. Higuchi, H. Abe, T. Ohsaki, J. Electrochem. Soc. 146 (1999) 2784.